

## Entrance and exit channel phenomena in $d$ - and $^3\text{He}$ -induced preequilibrium decay

H. H. Bissem, R. Georgi,\* and W. Scobel

*I. Institut für Experimentalphysik, Universität Hamburg, Hamburg, Federal Republic of Germany*

J. Ernst, M. Kaba, J. Rama Rao, and H. Strohe

*Institut für Strahlen- und Kernphysik der Universität Bonn, Bonn, Federal Republic of Germany*

(Received 24 January 1980)

Activation techniques were used to measure more than 30 excitation functions for single and multiple nucleon and/or  $\alpha$  particle emission for  $d + {}^{64,66}\text{Zn}$ ,  ${}^{89}\text{Y}$  with  $E_d = 9\text{--}26$  MeV and  ${}^3\text{He} + {}^{63,65}\text{Cu}$ ,  ${}^{93}\text{Nb}$  with  $E(^3\text{He}) = 10\text{--}44$  MeV. The excitation functions are generally in agreement with the results of a combined equilibrium and preequilibrium hybrid model calculation applying initial exciton numbers  $n_0 = 3$  for  $d$  and  $n_0 = 4$  for  ${}^3\text{He}$  reactions. The composite system  ${}^{66}\text{Ga}$  has been produced via  $d + {}^{64}\text{Zn}$  and  ${}^3\text{He} + {}^{63}\text{Cu}$  at excitation energies between 22 and 36 MeV. An entrance channel dependence shows up in the yields for single  $p$ - and  $n$ -emission when compared in the double ratio  $R = [\sigma(^3\text{He}, p)/\sigma(^3\text{He}, n)]/[\sigma(d, p)/\sigma(d, n)]$ . It approaches a value of about 2, indicating enhanced  $p$  emission for the  ${}^3\text{He}$ -induced reaction. This value disagrees with the equilibrium isospin formalism and is best reproduced by initial particle exciton numbers  $n_{0p} = n_{0n} = 1.5$  for  $d$  and  $n_{0p} = 2.5$ ,  $n_{0n} = 1.5$  for  ${}^3\text{He}$  projectiles, indicating conservation of charge asymmetry in the entrance channel. Isomeric ratios have been measured for  ${}^{89}\text{Y}(d, 2n){}^{89}\text{Zr}$  and  ${}^{93}\text{Nb}({}^3\text{He}, xn){}^{96-x}\text{Tc}$  ( $x = 1, 2, 3$ ). Calculations with a full statistical model fail to reproduce  $\sigma_g/\sigma_m$  as well as  $\sigma_g$  and  $\sigma_m$  for reasonable values of the spin cutoff parameter. Inclusion of a preequilibrium decay mode improves the fit, in particular if the angular momentum depletion of the composite system due to preequilibrium decay is increased over that of the equilibrium decay at the same channel energy.

NUCLEAR REACTIONS  ${}^{64,66}\text{Zn}$ ,  ${}^{89}\text{Y}(d, xnypz\alpha)$ ,  $E_d = 9\text{--}26$  MeV,  ${}^{63,65}\text{Cu}$ ,  ${}^{93}\text{Nb}({}^3\text{He}, xnypz\alpha)$ ,  $E_{^3\text{He}} = 10\text{--}44$  MeV,  $x \leq 4$ ,  $y \leq 1$ ,  $z \leq 2$ ; measured  $\sigma(E)$  by activation, enriched targets. Statistical model analysis including preequilibrium decay, deduced reaction mechanism, charge asymmetry conservation, spin depletion.

### I. INTRODUCTION

In recent years, the study of *proton* and *alpha* induced reactions was the main source of information for preequilibrium (PE) phenomena in nuclear reactions. For their interpretation a variety of reaction models have been developed<sup>1</sup> which well account for the hard component of the continuous energy spectra of nucleon and complex particle emission, the strongly forward peaked angular distributions, and the high energy tails of excitation functions for nucleon emission. The validity of these models for reactions induced by loosely bound projectiles like the  $d$  and  ${}^3\text{He}$  particle has been less intensively investigated since for these projectiles transfer and breakup reactions have to be considered, too.

In a first independent and later on joint effort, the present authors at the Bonn and Hamburg cyclotrons aimed to close this gap by studying excitation functions for  $d$ - and  ${}^3\text{He}$ -induced reactions on some medium weight nuclei between  $A \sim 60$  and  $90$ .<sup>2-4</sup> The experimental procedure is described in Sec. II. Essentially three lines were followed in the analysis of the data:

(1) *General behavior of the measured excitation functions.* We study in Sec. III to what extent the simple Weisskopf-Ewing (WE) and a more detailed Hauser-Feshbach (HF) model describe the data for the reactions  ${}^{63,65}\text{Cu}$ ,  ${}^{93}\text{Nb} + {}^3\text{He}$ , and  ${}^{89}\text{Y} + d$  without and with the inclusion of PE nucleon emission.

(2) *Entrance channel phenomena.* Inspired by the historical experiment of Ghoshal<sup>5</sup> investigating the decay of the composite system  ${}^{64}\text{Zn}^*$  formed through the entrance channels  ${}^{63}\text{Cu} + p$  and  ${}^{60}\text{Ni} + \alpha$ , we looked for a similar system for  $d$ - and  ${}^3\text{He}$ -induced reactions: Its decay should yield radioactive daughter nuclides following the emission of a single proton or neutron. The rather unique composite system fulfilling this condition is  ${}^{66}\text{Ga}^*$ . It can be formed by the entrance channels  ${}^{64}\text{Zn} + d$  ( $S_d = 10.85$  MeV) and  ${}^{63}\text{Cu} + {}^3\text{He}$  ( $S_{^3\text{He}} = 13.07$  MeV). We observed the decay of  ${}^{66}\text{Ga}^*$  between 22 and 36 MeV excitation energy where the emission of a single nucleon is dominated by noncompound processes. In Sec. IV we investigate to what extent the relative branching of the total reaction cross section to the final evaporation residues depends on the entrance

channel, how much proton emission is enhanced over neutron emission in the  $^3\text{He}$ -induced reaction, and whether or not this is related to the different charge asymmetries in the  $^3\text{He}$  and  $d$  projectiles.

(3) *Isomeric cross section ratios.* The proximity of the  $(1g_{9/2}\pi)$  and  $(2p_{1/2}\pi)$  states near  $A = 90$  leads to longlived isomers in many of the residual nuclei which were reached by the  $^{89}\text{Y} + d$  and  $^{93}\text{Nb} + ^3\text{He}$  reactions. The study of isomeric ratios with a Hauser-Feshbach model extended to include a PE decay mode should reveal informa-

tion on the spin distribution in the residual system due to the nonequilibrium processes involved (Sec. V).

Nonequilibrium contributions to the excitation functions under consideration are not necessarily due to PE decay, although PE decay models may include direct interaction contributions<sup>1,6</sup>; therefore a short section (Sec. VI) is devoted to the question of further competing reaction mechanisms. The conclusions drawn from this work are presented in Sec. VII.

TABLE I. Reactions under investigation and  $\gamma$  lines used for identification. The laboratory (BN or HH), number  $N$  of data points of the excitation function, maximum projectile energy  $E$ , and maximum energy degradation  $\Delta E$  are given in the last columns.

Reaction	$T_{1/2}$	$E_\gamma$ (keV)	$I_\gamma$	Lab	$N$	$E$ (MeV)	$\Delta E$ (MeV)
$^{63}\text{Cu}(^3\text{He}, n)^{65}\text{Ga}$	15.2 min	115; 153; 752	0.532; 0.087; 0.08	BN	5	24.8	11
				HH	14	31.7	0
$^{63}\text{Cu}(^3\text{He}, n + p)^{65}\text{Zn}$	243.8 d	1116	0.498	BN	5	24.8	11
$^{63}\text{Cu}(^3\text{He}, 2n)^{64}\text{Ga}$	2.6 min	809; 992	0.14; 0.46	HH	15	35.0	0
$^{63}\text{Cu}(^3\text{He}, 3n + p2n)^{63}\text{Zn}$	38.8 min	670; 962	0.0883; 0.0695	BN	5	24.8	11
				HH	17	42.5	0
$^{63}\text{Cu}(^3\text{He}, \alpha n)^{64}\text{Cu}$	3.41 h	283; 656	0.13; 0.096	BN	5	24.8	11
$^{63}\text{Cu}(^3\text{He}, 2\alpha)^{58}\text{Co}$	71.3 d	811	0.994	BN	5	24.8	11
$^{65}\text{Cu}(^3\text{He}, n)^{67}\text{Ga}$	78.0 h	93.3	0.70	HH	16	43.8	9
$^{65}\text{Cu}(^3\text{He}, 2n)^{66}\text{Ga}$	9.4 h	834; 1039	0.059; 0.373	HH	23	43.8	9
$^{65}\text{Cu}(^3\text{He}, 3n)^{65}\text{Ga}$	15.2 min	115; 153	0.532; 0.087	HH	20	41.4	0
$^{65}\text{Cu}(^3\text{He}, 4n)^{64}\text{Ga}$	2.6 min	992; 1387	0.46; 0.14	HH	4	41.7	0
$^{64}\text{Zn}(d, n)^{65}\text{Ga}$	15.2 min	115; 153; 752	0.532; 0.087; 0.08	BN	7	26.7	15
$^{64}\text{Zn}(d, n + p)^{65}\text{Zn}$	243.8 d	1116	0.498	BN	6	26.7	16
$^{64}\text{Zn}(d, 2n)^{64}\text{Ga}$	2.6 min	809; 992	0.14; 0.46	BN	6	23.9	14
$^{64}\text{Zn}(d, 3n + p2n)^{63}\text{Zn}$	38.4 min	670; 962	0.883; 0.0695	BN	7	25.8	14
$^{64}\text{Zn}(d, \alpha n)^{61}\text{Cu}$	3.41 h	283; 656	0.13; 0.096	BN	6	23.9	14
$^{64}\text{Zn}(d, 2\alpha)^{58}\text{Co}$	71.3 d	811	0.994	BN	5	25.8	15
$^{66}\text{Zn}(d, 2n)^{66}\text{Ga}$	9.4 h	834; 1039	0.059; 0.373	BN	5	25.8	5
$^{66}\text{Zn}(d, 3n)^{65}\text{Ga}^a$	15.2 min	115; 153; 752	0.532; 0.087; 0.08	BN	3	25.8	3
$^{66}\text{Zn}(d, 3n + p2n)^{65}\text{Zn}^a$	243.8 d	1116	0.498	BN	3	25.8	5
$^{89}\text{Y}(d, p)^{90}\text{Y}^m$	3.19 h	203; 483	0.965; 0.90	BN	8	25.9	15
$^{89}\text{Y}(d, 2n)^{89}\text{Zr}^e$	78.4 h	909	0.99	BN	10	25.9	20
$^{89}\text{Y}(d, 2n)^{89}\text{Zr}^m$	4.18 min	588	0.93	BN	8	25.9	15
$^{89}\text{Y}(d, 3n)^{88}\text{Zr}$	85 d	393	0.97	BN	8	25.9	6
$^{89}\text{Y}(d, p2n)^{88}\text{Y}$	107 d	1836	0.994	BN	4	25.9	6
$^{89}\text{Y}(d, p3n)^{87}\text{Y}^m$	14 h	381	0.74	BN	3	25.9	2
$^{89}\text{Y}(d, \alpha)^{87}\text{Sr}^m$	2.8 h	388	0.83	BN	8	25.9	15
$^{93}\text{Nb}(^3\text{He}, n)^{95}\text{Tc}^m$	61 d	204	0.803	BN	11	30	21
$^{93}\text{Nb}(^3\text{He}, n)^{95}\text{Tc}^e$	20 h	766	0.94	BN	10	30	21
				HH	12	42.8	9
$^{93}\text{Nb}(^3\text{He}, 2n)^{94}\text{Tc}^m$	52 min	871	0.94	HH	15	42.8	9
$^{93}\text{Nb}(^3\text{He}, 2n)^{94}\text{Tc}^e$	293 min	703; 850; 871	0.998; 0.977; 1.0	HH	15	42.8	9
$^{93}\text{Nb}(^3\text{He}, 3n)^{93}\text{Tc}^m$	43.0 min	390	0.63	HH	16	42.8	9
$^{93}\text{Nb}(^3\text{He}, 3n)^{93}\text{Tc}^e$	2.75 h	1363; 1521	0.67; 0.25	HH	13	42.8	9
$^{93}\text{Nb}(^3\text{He}, 4n)^{92}\text{Tc}$	4.4 min	148	0.55	HH	7	42.8	0

<sup>a</sup> Used to correct for the  $^{66}\text{Zn}$  impurity in the  $^{64}\text{Zn}$  target (see Table II).

## II. EXPERIMENTAL PROCEDURE

The excitation functions listed in Table I were measured with activation techniques. The irradiations were performed at the Bonn (BN) and the Hamburg (HH) isochronous cyclotrons, respectively. Self-supporting metallic foils of high purity and isotopic enrichment (see Table II) were activated in most cases in combination with energy degrading foils (of aluminum, and of yttrium for  $^{89}\text{Y} + d$ ) as foil stacks. Projectile energies and the maximum energy degradation  $\Delta E$  within a stack were calculated from the tables of Williamson *et al.*<sup>7</sup> The uncertainty in energy after degradation of  $^3\text{He}$  from 25 to 10 MeV, for example, was calculated<sup>8</sup> to be about  $\pm 0.95$  MeV full width at half maximum (FWHM). Single foil activation was applied to reactions leading to residual nuclei with short half-lives ( $T_{1/2} \lesssim 40$  min) either by tuning the cyclotron to the projectile energy under consideration or with a fixed projectile energy by placing the target behind an energy degrader. These irradiations were performed with currents in the order of 200 nA extending over  $\sim 5$  min, whereas the longer half-life components were activated for 2–10 h.

In both experiments the irradiations were performed in reaction chambers designed to allow the direct determination of beam current by integration of the charge collected in a Faraday cup. In cases where the total irradiation time was comparable with the half-life of a nuclide under investigation, the variation of the current in time was accounted for by a technique developed for neutron activation.<sup>9</sup>

After irradiation the samples were placed in front of a coaxial Ge (Li) detector of 77 cm<sup>3</sup> (69 cm<sup>3</sup>) active volume and a resolution of 2.43 keV (2.3 keV) at  $E_\gamma = 1332$  keV. Signals were handled with conventional electronics and accumulated into 4000 channel analyzer arrays. The pulse height spectra were stored on magnetic tape mostly 3–4 times per half-life and sample. A reference pulser was fed into the signal line for accurate dead-time correction.

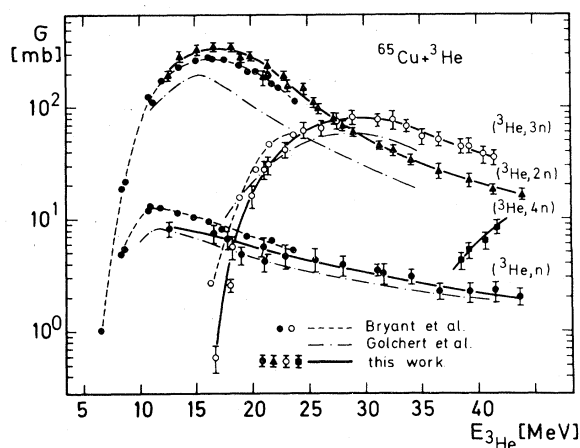


FIG. 1. Experimental excitation functions for the  $^{65}\text{Cu}(^3\text{He}, xn)$  reactions ( $x=1-4$ ) and comparison to those of the literature (Refs. 14 and 15).

The peak integrals were obtained from the pulse height spectra with multiple line fit programs including linear background and exponential tailing corrections.<sup>2-4</sup> Additional corrections for recoiling residual nuclei that leave or enter the target foil were not applied, because their ranges are in the order of 300  $\mu\text{g}/\text{cm}^2$  and less,<sup>10</sup> i.e., small compared with the thickness of the target foils. The half-lives and  $\gamma$  energies used for identification as well as the branching ratios  $I_\gamma$  are given in Table I and are collected from.<sup>11-13</sup>

The efficiencies of the detectors were determined by means of calibrated  $\gamma$  sources (BN:  $^{58}\text{Co}$ ,  $^{60}\text{Co}$ ,  $^{88}\text{Y}$ ,  $^{152}\text{Eu}$ ,  $^{182}\text{Ta}$ ; HH:  $^{22}\text{Na}$ ,  $^{54}\text{Mn}$ ,  $^{57}\text{Co}$ ,  $^{60}\text{Co}$ ,  $^{137}\text{Cs}$ ). The calibration points were used to interpolate best fitting efficiency curves  $\eta(E_\gamma)$  from a  $\log \eta$  vs  $\log E_\gamma$  presentation (BN), and from Monte Carlo calculations performed on the basis of the geometrical data of the x-rayed and  $\gamma$ -scanned detector (HH).

In Fig. 1 the resulting excitation functions for the  $^{65}\text{Cu} + ^3\text{He}$  reaction are compared with previous measurements by Bryant *et al.*<sup>14</sup> and Golchert *et al.*<sup>15</sup> Within the experimental errors the data are in agreement except for the case of

TABLE II. Target specifications.

Target	Thickness (mg/cm <sup>2</sup> )	Enrichment (%)	Major impurities (%)
$^{63}\text{Cu}$	4.95–10.37	99.9	$^{65}\text{Cu}$ (0.1)
$^{65}\text{Cu}$	5.41–11.14	99.8	$^{63}\text{Cu}$ (0.2)
$^{64}\text{Zn}$	9.54–11.18	98.6	$^{66}\text{Zn}$ (0.8), $^{68}\text{Zn}$ (0.5)
$^{66}\text{Zn}$	9.64–10.47	96.9	$^{64}\text{Zn}$ (1.5), $^{68}\text{Zn}$ (0.9)
$^{89}\text{Y}$	11.10 and 47.14	100	
$^{93}\text{Nb}$	4.62, 11.0, and 22.4	>99.9	Ta(0.05), Fe(0.01)

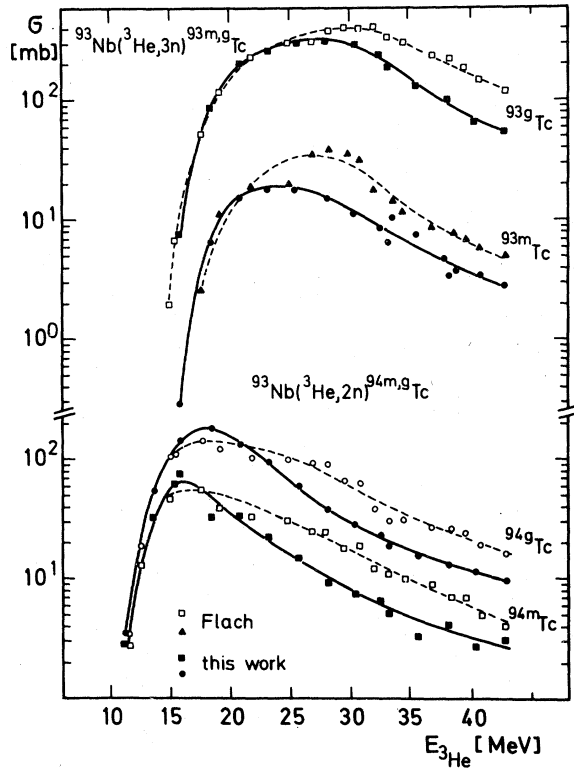


FIG. 2. Measured excitation function for the  $^{93}\text{Nb}(^3\text{He}, xn)^{96-x}\text{Tc}^{m,g}$  reactions ( $x=2, 3$ ) and comparison with the work of Flach (Ref. 10).

$^{65}\text{Cu}(^3\text{He}, 2n)$  where we find a yield twice as large. A similar discrepancy is observed for the case of the  $^{93}\text{Nb}(^3\text{He}, xn)^{93,94}\text{Tc}^{m,g}$  reaction with respect to the data of Flach<sup>10</sup> which remains unexplained since the same spectroscopic data were used (Fig. 2). The other excitation functions will be presented in the next section. Their absolute values show errors of  $\pm 8$ – $10\%$  (BN) and  $\pm 10$ – $20\%$  (HH). These quotations include uncertainties due to counting statistics, photo peak integration, target thickness, current integration, recoiling residual nuclei, and detector efficiency, but not those of the  $\gamma$  spectroscopic data given in Table I. All excitation functions are available in tabular form on request.

### III. ANALYSIS IN TERMS OF EQUILIBRIUM AND PREEQUILIBRIUM MODELS

#### A. Equilibrium emission models

Before discussing the effects of preequilibrium particle emission it is interesting to compare part of the data with existing equilibrium model predictions. The WE approach<sup>16</sup> is incorporated in the widely used code OVERLAID ALICE.<sup>17</sup> It

allows computation of the emission of up to 20 nucleons in a deexcitation cascade. The following input parameters were used: (i) The particle separation energies were taken from the tables of Wapstra and Gove<sup>18</sup>; (ii) reaction cross sections and inverse cross sections were calculated from optical model (OM) transmission coefficients. For  $p$ ,  $n$ , and  $^3\text{He}$  particles the OM parameters of Becchetti and Greenlees<sup>19,20</sup> were used, for  $\alpha$  particles those of McFadden and Satchler<sup>21</sup>; (iii) the level density expression  $\rho(U) = \text{const} \times U^{-2} \exp[2(aU)^{1/2}]$  with  $a = (A_{\text{target}} + A_{\text{projectile}}) / 8 \text{ MeV}^{-1}$  was applied to all nuclei in the decay cascade. No pairing corrections were introduced.

In Fig. 3 the WE calculations are compared with the experimental data for  $^{63}\text{Cu} + ^3\text{He}$ . For the  $2n$  emission and the sum of the  $3n$  and  $p2n$  emissions, the rising parts of the excitation functions as well as the height of the maxima are quite well described. Also shown are curves computed with the separation energies of Myers and Swiatecki<sup>22</sup> which are calculated from the liquid drop model including shell corrections without pairing. Since the reaction thresholds are generally less well reproduced, this option was abandoned further on. Also shown in Fig. 3 as well as in Figs. 5 and 6 are the predictions of the more sophisticated statistical code of Uhl<sup>23</sup> taking full account of angular momentum effects and  $\gamma$ -ray competition. In addition to the input data (i) and (ii) this code applies a back-shifted Fermi-gas level density (for details see Sec. V). Generally, these calculations reproduce reaction thresholds well and predict a somewhat flatter decrease of the yield to higher energies. However, the absolute height of the excitation func-

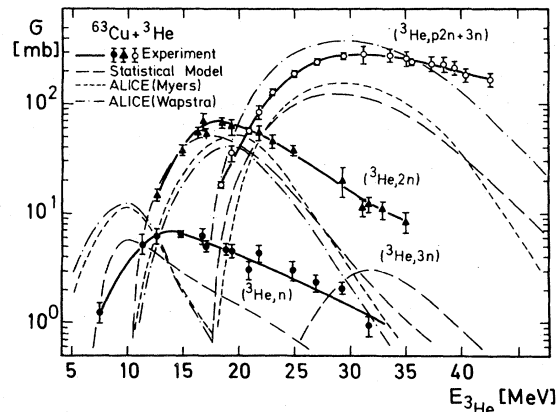


FIG. 3. Measured excitation functions for the  $^{63}\text{Cu} + ^3\text{He}$  reactions and comparison with the full statistical model of Uhl (Ref. 23) and two Weisskopf-Ewing calculations (Ref. 16) using the code OVERLAID ALICE (Ref. 17) with binding energies of Myers and Swiatecki (Ref. 22) and those of Wapstra and Gove (Ref. 18) (see text).

tions is reproduced with about the same degree of accuracy as with the simpler WE model. Neither approach can explain the flat high energy tails. Here, a mechanism for a fast cooling of the primary composite system is needed: the emission of more energetic preequilibrium particles.

### B. Preequilibrium emission

For the investigation of PE phenomena the hybrid model<sup>24</sup> was used. It has been successfully applied to a variety of light particle induced reactions and should serve as a good approximation of an overall estimate of nonequilibrium processes (see Sec. VII). Differences between this and other approaches e.g., the exciton model of Gadioli *et al.* are noted in Ref. 25 and are explicitly discussed in Refs. 26 and 27. All calculations were performed with the OVERLAID ALICE code.<sup>17</sup> Multiple preequilibrium emission was not taken into account. In addition to the input parameters specified in Sec. III A the following quantities enter into the PE part of the program: (iv) The nucleon-nucleon collision rate was calculated from the mean free path of nucleons in nuclear matter; (v) the density of particles per MeV in an  $n$ -exciton state containing  $p$  particles and  $h$  holes was calculated from the expressions of Ericson,<sup>28</sup> however, modified for a limited potential depth of 40 MeV.<sup>1,17</sup> Starting with an initial exciton number  $n_0 = p_0 + h_0$  the exciton number is increased by 2 in each step of the deexcitation cascade. The depletion due to PE emission of previous stages is taken into account. Any charge asymmetry of the projectile may be reflected in different initial particle numbers  $p_{0p}$  and  $p_{0n}$  for protons and neutron, respectively. Their value is increased in each step of the relaxation process by 0.5. Hence the only free set of fit parameters are the initial exciton numbers  $n_0(p_{0n}, p_{0p})$  with  $p_0 = p_{0n} + p_{0p}$  and  $h_0 = n_0 - p_0$ .

In Figs. 4–7 the experimental excitation functions for  $^{63,65}\text{Cu}$ ,  $^{93}\text{Nb} + ^3\text{He}$ , and  $^{89}\text{Y} + d$  are compared with the theoretical predictions for the indicated sets of  $n_0(p_{0n}, p_{0p})$ . In Fig. 4 the curves for  $^{63}\text{Cu} + ^3\text{He}$  clearly demonstrate the improvement obtained by the inclusion of PE emission. In particular, the flatter falloff of the high energy tails for  $n$  and  $2n$  emissions is better reproduced than by the equilibrium code (cf. Fig. 3). At the high energy end the  $n_0 = 5$  curves tend to decrease steeper than do the experimental data. Yet it is apparent that only the excitation functions for one or two nucleon emission are sensitive enough to the choice of  $n_0$  while for more nucleons an extended projectile energy

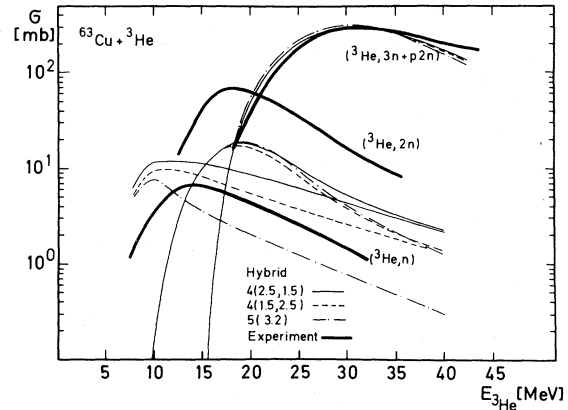


FIG. 4. Comparison of the experimental excitation functions  $^{63}\text{Cu} + ^3\text{He}$  with the hybrid model (Ref. 24) using the code OVERLAID ALICE (Ref. 17) for the initial exciton numbers  $n_0(p_{0n}, p_{0p})$  indicated.

range is needed. From the  $^{63,65}\text{Cu}$  data alone, no definite conclusion on the best initial proton to neutron ratio can be drawn, though the single neutron emission seems to be most sensitive (see Sec. IV). For  $^3\text{He}$  particles the generally adopted set is 4(1.5, 2.5). Corresponding curves for the case of  $^{93}\text{Nb} + ^3\text{He}$  are displayed in Fig. 6; it also contains the results of a geometry dependent hybrid model (GDH) calculation<sup>1,17</sup> where the average nuclear density along classical projectile trajectories is taken into account. In individual calculations for each partial wave, this  $l$ -dependent density enters into the single particle state density, the Fermi energy, and the nuclear collision rate. In further analysis we stick to the simpler hybrid model, since in the present cases the GDH calculations do not improve the fit to the experimental data.

The strong discrepancy of all theoretical curves for the  $^{93}\text{Nb}(^3\text{He}, 4n)^{92}\text{Tc}$  reaction originates from

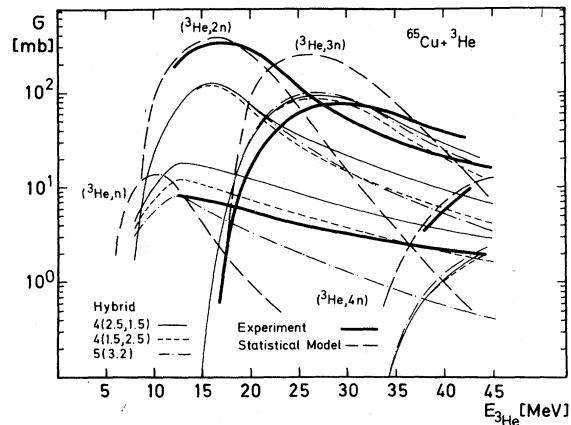


FIG. 5. Same as Fig. 4 for  $^{65}\text{Cu} + ^3\text{He}$ .

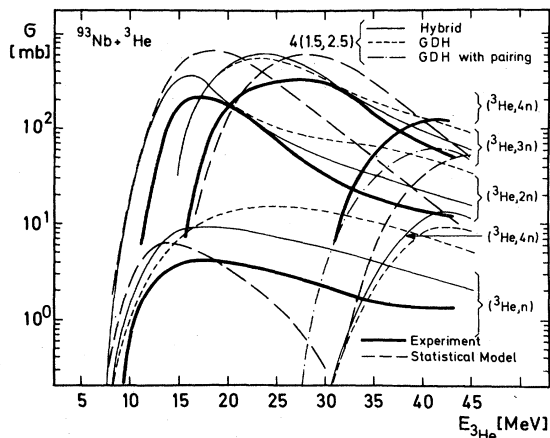


FIG. 6. Same as Fig. 4 for  $^{93}\text{Nb} + {}^3\text{He}$ . In addition, the predictions of the geometry dependent hybrid model (GDH) are shown as well as those of the full statistical model of Uhl (Ref. 23). The GDH calculation with pairing for the  $({}^3\text{He}, 4n)$  reaction is explained in the text.

the neglect of pairing and shell effects in the level density calculation. Since the separation energy of the fourth neutron from the closed shell ( $N=50$ ) nucleus  $^{93}\text{Tc}$  is especially high (12.8 MeV) while the proton separation energy is rather small (4.1 MeV), the population of the doubly odd nu-

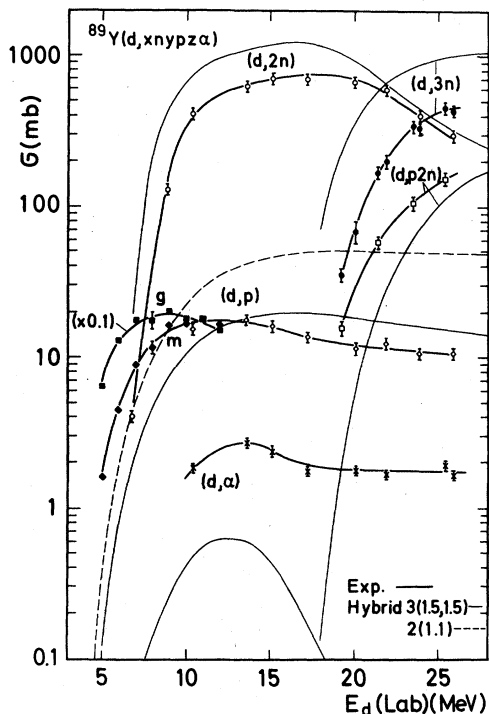


FIG. 7. Same as Fig. 4 for  $^{89}\text{Y} + d$ . The experimental yields are connected by smooth curves to guide the eye. The data points marked  $\blacksquare$  and  $\blacklozenge$  were taken from Ref. 29.

cleus  $^{92}\text{Tc}$  is considerably affected by this neglect of pairing effects.

The inclusion of pairing corrected separation energies for the emission of a fourth particle removes this discrepancy (see Fig. 6). However, taken as a general recipe, this procedure leads to unphysical shifts of subsequent reaction thresholds.

Similar observations can be made for the  $d$ -induced reactions on  $^{89}\text{Y}$  (Fig. 7). The experimental results are compared with hybrid model calculations using the initial exciton numbers 3(1.5, 1.5). At the evaporation peak the  $(d, 2n)$  curve is overestimated by the theory by nearly a factor of 2, the  $(d, 3n)$  curve by about a factor 3, while the  $(d, p2n)$  reaction is much stronger than predicted. Also here the population of the doubly even nucleus  $^{88}\text{Zr}$  is overestimated in contrast to the doubly odd nucleus  $^{88}\text{Y}$ . Again, the exciton number dependence of PE decay shows up strongly only in the theoretical curves for single nucleon emission i.e., for the  $^{89}\text{Y}(d, p)^{90}\text{Y}$  excitation functions with  $n_0 = 2$  and 3 in Fig. 7. At higher energies the data for populating the  $7^+$  isomer in  $^{90}\text{Y}$  are reproduced quite well by the curve with  $n_0 = 3$ . At our bombarding energies the high spin isomer should be populated much more than the  $2^-$  g.s. However, as found by Riley *et al.*<sup>29</sup> the g.s. of  $^{90}\text{Y}$  is fed about one order of magnitude more than is the isomer, a fact which is explained by the dominance of stripping reactions to mainly low spin states (see Sec. V). The low spin isomer of  $^{87}\text{Sr}^m(\frac{1}{2}^-)$  is less strongly populated and shows a flat high energy tail while the theoretical curve falls off steeply due to the neglect of preequilibrium  $\alpha$  emission in the OVERLAID ALICE code.

#### IV. ENTRANCE CHANNEL PHENOMENA

The composite system  $^{66}\text{Ga}^*$  was formed through the entrance channels  $^{64}\text{Zn} + d$  and  $^{63}\text{Cu} + {}^3\text{He}$  (see Table I) at excitation energies where the preequilibrium emission dominates the emission of the first particle out. The  $(2n)$  decay of  $^{66}\text{Ga}^*$  formed in the reactions  $^{66}\text{Zn} + d$  and  $^{65}\text{Cu} + {}^3\text{He}$  (see Table I) was studied in a similar way. For a better comparison, the experimental and theoretical evaporation residue yields were normalized to the optical model reaction cross section; thus the influence of the Coulomb barriers of the respective entrance channels is removed, and entrance channel effects show up more clearly.

##### A. Decay of $^{66,68}\text{Ga}^*$

The normalized excitation functions as a func-

tion of the excitation energy in the composite systems  $^{66,68}\text{Ga}^*$  are displayed in Figs. 8–11. If isospin effects and small differences in the angular momentum distribution in the entrance channel are neglected, both kinds of projectiles should lead to the same normalized yields, assuming a pure compound nucleus reaction. In preequilibrium processes the influence of different initial exciton numbers for  $d$ - and  $^3\text{He}$ -induced reactions should show up.

For single nucleon emission yields this feature is clearly observed (Fig. 8). The  $n$  and  $(n+p)$  curves follow quite well the hybrid model predictions with  $n_0(d)=3$  and  $n_0(^3\text{He})=4$ . The remaining deviations are attributed to the simplifying assumptions entering the hybrid model code as already discussed in Sec. III. It is to be noted that, different from input (ii) in Sec. III A, the inverse cross sections were computed from a subroutine provided with the OVERLAID ALICE code.<sup>17</sup>

For single nucleon emission, improved fits are obtained while the theoretical yields for multi-nucleon emission are hardly changed (cf. Figs. 4, 8 and 9 and Figs. 5 and 10). For  $^{64}\text{Zn}+d$  the theoretical curves for  $n$  and  $(n+p)$  emission de-

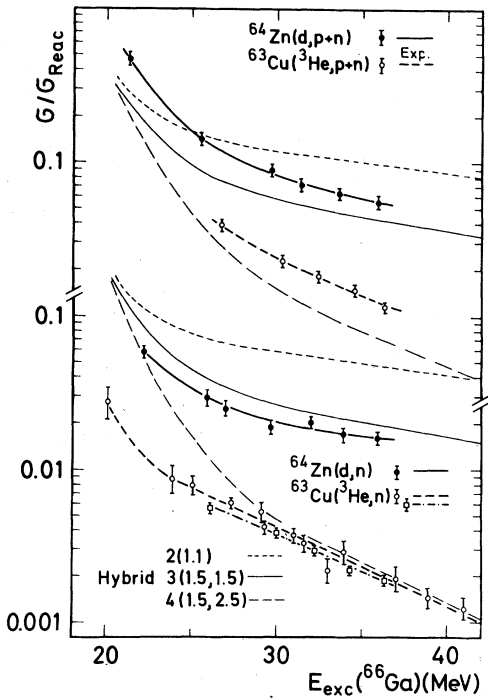


FIG. 8. Comparison of experimental and calculated normalized yields for  $n$  and  $(p+n)$  emission from the composite system  $^{66}\text{Ga}^*$  formed in the reactions  $^{64}\text{Zn}+d$  and  $^{63}\text{Cu}+^3\text{He}$ . The  $(^3\text{He},n)$  data points marked  $\square$  are taken from set BN (cf. Table I).

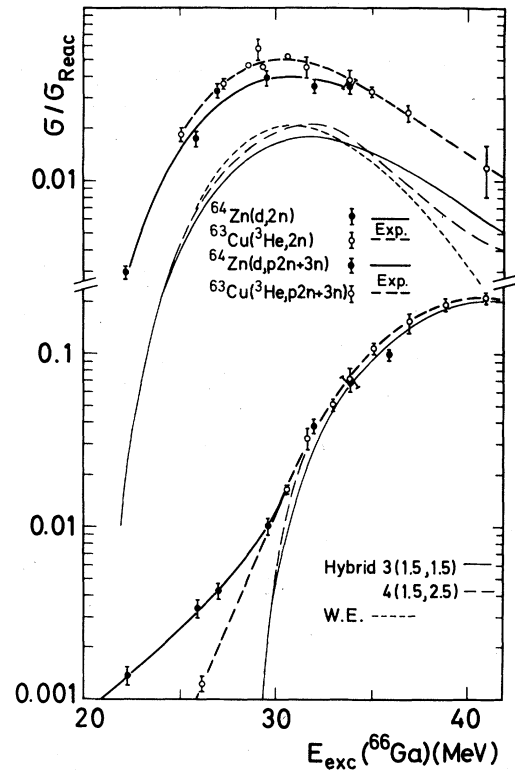


FIG. 9. Same as Fig. 8 for the  $2n$  and  $(3n+p2n)$  emissions from  $^{66}\text{Ga}^*$ . For the  $2n$  process also the prediction of the Weisskopf-Ewing (WE) model is displayed.

viate from the experimental ones by a constant factor while for low excitations the experimental  $^{63}\text{Cu}+^3\text{He}$  curves rise less steeply than the OM calculated branchings. One reason for this may be the too large reaction cross sections at low bombarding energies (20 MeV excitation in  $^{66}\text{Ga}^*$  corresponds to 7.5 MeV) while the uncertainties of OM predictions do not enter in the theoretical curves. The optimal splitting of the initial par-

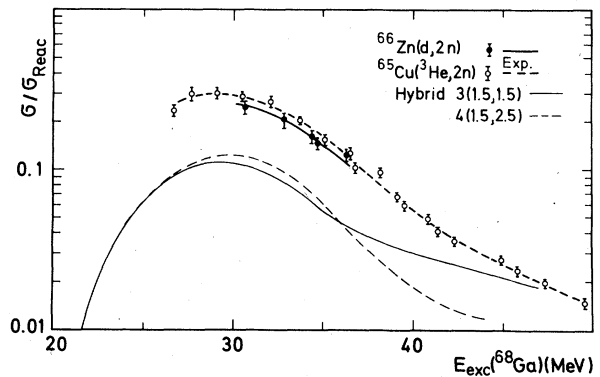


FIG. 10. Same as Fig. 8 for the  $2n$  emission from the composite system  $^{68}\text{Ga}^*$ .

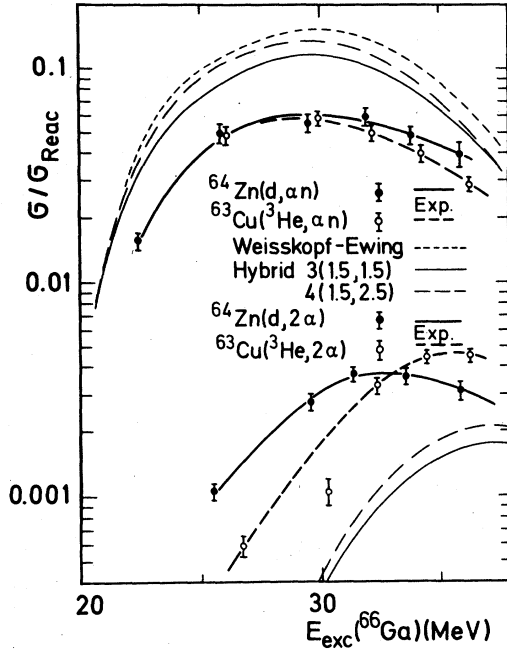


FIG. 11. Same as Fig. 8 for the  $(\alpha n)$  and  $(2\alpha)$  emissions from  $^{66}\text{Ga}^*$ . For the  $(\alpha n)$  process the prediction of the Weisskopf-Ewing model is also given.

Exciton number  $p_0$  into initial proton and neutron numbers  $p_{0p}$  and  $p_{0n}$  cannot be deduced from the quality of individual fits alone since curves for different ratios  $p_{0p}/p_{0n}$  are almost parallel (see Figs. 4 and 5). A more sensitive procedure is developed in Sec. IV B. The optimal initial exciton numbers are indicated in Figs. 8–11. Both curves for  $n$  emission and  $(n+p)$  emission differ from the hybrid model predictions by about the same factor in each case. While  $n$  emission is overestimated,  $p$  emission is clearly underestimated.

## B. Conservation of projectile charge asymmetry

### 1. General considerations

As shown in Sec. III B, the excitation functions for single nucleon emission are the most sensitive probes for determining not only the initial exciton number  $n_0$ , but also the initial number of protons  $p_0$  and neutrons  $p_{0n}$ . The ambiguities in fitting these data are minimized by comparing not single excitation functions, but the calculated double ratio

$$R(E_{\text{exc}}) = \sigma(^3\text{He}, p) / \sigma(^3\text{He}, n) : \sigma(d, p) / \sigma(d, n) \quad (1)$$

with the corresponding experimental value

$$R[E_{\text{exc}}(^{66}\text{Ga}^*)] = \frac{\sigma(^3\text{He}, p+n) - \sigma(^3\text{He}, n)}{\sigma(^3\text{He}, n)} : \frac{\sigma(d, p+n) - \sigma(d, n)}{\sigma(d, n)} \quad (2)$$

For two-particle emission [e.g.,  $(2n)$  in Figs. 9 and 10, and  $(\alpha n)$  in Fig. 11] the influence of the initial exciton number is already rather weak. Hence, the reduced yields for  $d$ - and  $^3\text{He}$ -induced reactions nearly coincide and cross at about the same excitation energies as the theoretical curves. The initial exciton number dependence shows up only at the high energy tails; e.g., in Figs. 9 and 10 the  $(^3\text{He}, 2n)$  data rather follow the curves for  $n_0=4$  than those for  $n_0=3$ .

From the systematics of binding energies and Coulomb barriers it is deduced that for the population of  $^{61}\text{Cu}$  by the  $(\alpha, n)$  process, first a preequilibrium neutron is emitted followed by an equilibrium  $\alpha$  particle. Only at the higher bombarding energies might first chance preequilibrium  $\alpha$  emission play a more important role. This seems to be indicated in Fig. 11 by an experimental falloff which is flatter than shown by the theoretical  $(\alpha n)$  curves, which do not include preequilibrium  $\alpha$  emission. As deduced from  $Q$  value arguments, the only reaction leading to  $^{58}\text{Co}$  which is energetically allowed is the  $(2\alpha)$  emission. As shown in Fig. 11, the two experiments differ more strongly from each other than the theoretical curves for pure equilibrium  $\alpha$  emission, indicating a stronger nonequilibrium process for  $d$  than for  $^3\text{He}$ -induced reactions.

Finally, the emission of three nucleons is observed as the sum of the  $(3n)$  and  $(p2n)$  reactions leading to  $^{63}\text{Zn}$  (Fig. 9). At the high excitation energies the data actually coincide with the model predictions, but below 30 MeV excitation the theory underestimates the experiments by more than an order of magnitude. Apparently, reactions having lower  $Q$  values [e.g., inelastic processes like  $(d, dn)$ , breakup reactions like  $(^3\text{He}, dn)$ , and transfer and charge exchange reactions like  $(d, t)$  and  $(^3\text{He}, t)$ ] do contribute (cf. Sec. VI).

Naively, one would expect that the ratio  $\sigma(^3\text{He}, p)/\sigma(^3\text{He}, n)$  is much larger than the corresponding ratio  $\sigma(d, p)/\sigma(d, n)$ , since the initial (active) exciton particles stem from the projectile, and the proton to neutron ratio is two for the  $^3\text{He}$  projectile but only one for the deuteron. The symmetry of the deuteron and the charge symmetry of the nuclear force demand symmetric particle numbers ( $p_{op}/p_{on}=1$ ) in the deexcitation cascade. For  $^3\text{He}$  this ratio is less well fixed *a priori*. Assuming a charge independent nuclear interaction in the first collision of a  $^3\text{He}$  nucleon with the target, one would expect  $n_0=4$ ,  $p_{op}=2.5$ , and  $p_{on}=1.5$ , i.e., the excited additional nucleon is equally likely to be a proton or a neutron. Assuming charge symmetry only with  $\sigma(np):\sigma(nn):\sigma(pp)=3:1:1$  one would get the particle configurations  $2 \times [3(p)^2(n)^2 + (p)^3(n)^1]$  and  $[(p)^2(n)^2 + 3(p)^3(n)^1]$  following the interactions of the protons or the neutron of  $^3\text{He}$ , respectively. Hence, almost the same result is obtained,  $p_{op} = \frac{29}{12} = 2.42$  and  $p_{on} = \frac{19}{12} = 1.58$ . On the other hand, one could argue that a quasiequilibrium holds in each stage of the relaxation process, i.e., initially all possible  $n_0=4$  exciton states are excited and  $p_{op}=p_{on}$ .

Hence, within the framework of current PE models<sup>1,26,27</sup> one may try to answer this question by investigating which initial exciton numbers fit the data best (method A).

Another, less empirical approach would be to check if the well developed theory of isospin conservation in compound nucleus reactions<sup>30</sup> may be extended to PE reactions. Suggestions and calculations along this line have been proposed by Chevarier *et al.*<sup>31</sup> and Kalbach-Cline *et al.*<sup>32</sup> In the next subsection we review this approach (method B). Finally, it is worth mentioning that a more thorough treatment of isospin in PE reactions has recently been published by Feinstein<sup>33</sup>; however, at present this theory does not allow computation of residual nucleus yields.

## 2. Model calculations of $R(E_{exc})$

*Method A (charge dependent initial exciton numbers).* In  $R(E_{exc})$  theoretical uncertainties in the optical model reaction cross section cancel and uncertainties in level densities due to pairing and shell effects should be diminished, leaving only a dependence on the exciton numbers. With the well established choice of  $n_0(d)=3$  and  $n_0(^3\text{He})=4$ ,  $R(E_{exc})$  in Eq. (1) strongly depends on the charge asymmetry of the initial exciton numbers  $p_{on}$  and  $p_{op}$  for  $^3\text{He}$ -induced reactions. From arguments of charge symmetry we put  $p_{on}=p_{op}=1.5$  in the deuteron. Hence—in short

notation—we get

$$R_A^{PE}(E_{exc}) = \frac{\sigma_p(4, p_{on}, p_{op})\sigma_n(3, 1.5, 1.5)}{\sigma_n(4, p_{on}, p_{op})\sigma_p(3, 1.5, 1.5)}. \quad (3)$$

*Method B (isospin formalism with  $p_{on}/p_{op}$ ).*

The basic ideas of the compound nucleus isospin formalism are illustrated in Fig. 12. The excitation energies  $\Delta E_{T^>}$  for the  $T^>$  g.s. were taken from Ref. 34. Assuming strict isospin conservation in  $d$ -induced reactions, one may only form  $T^<$  states in  $^{66}\text{Ga}^*$  due to the isospin Clebsch-Gordan coefficients  $C^2(d, <) = 1$  and  $C^2(d, >) = 0$ . For the  $^3\text{He}$  projectile, the corresponding coefficients are  $C^2(^3\text{He}, <) = \frac{5}{6}$  and  $C^2(^3\text{He}, >) = \frac{1}{6}$ . The isospin Clebsch-Gordan coefficients for  $p$ ,  $n$ , and  $\alpha$  particle emissions from the  $T^<$  and  $T^>$  states in  $^{66}\text{Ga}^*$  are indicated in Fig. 12. For a pure PE reaction populating only  $T^<$  states in the residual nuclei  $^{65}\text{Zn}$  and  $^{65}\text{Ga}$  (see Fig. 12) we get, with  $T_0$  being the g.s. isospin of the residual nucleus  $^{66}\text{Ga} - p = ^{65}\text{Zn}$ ,

$$R_B^{PE}(E_{exc}) = R_A^{PE} [1 + (2T_0)^{-2} \sigma_{p><}(4, 2, 2) / \sigma_{p<<}(4, 2, 2)]. \quad (4)$$

Here, the  $\sigma_{p><}$  ( $\sigma_{p<<}$ ) indicate PE transition yields from initial  $T^>$  ( $T^<$ ) states to the final  $T^<$  isospin states in the residual nuclei for the  $^3\text{He}$ -induced reaction with  $C^2=1$ , starting with equal probability for exciting protons or neutrons in the initial exciton state ( $p_{on}=p_{op}=2$ ). The term in brackets gives the enhancement of the  $^3\text{He}$ -induced reaction due to isospin conservation. In PE emission to the low lying states under consideration, the first stage contributes most, and any difference in depleting proton or neutron states due to isospin effects may be neglected. Hence, the ratio  $\sigma_{p><}/\sigma_{p<<} \sim (1 - E_{T^>}/E_{exc})^{-n_0+1}$

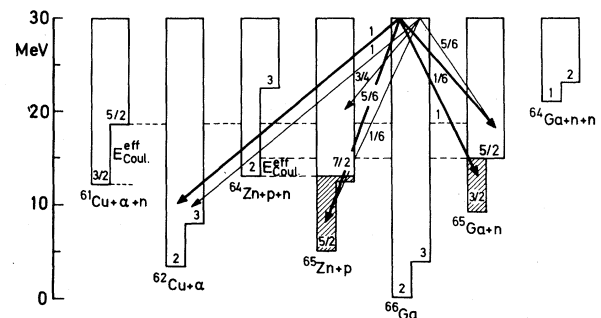


FIG. 12. Decay modes of the  $T^<$  (thick arrows) and  $T^>$  (thin arrows) states in  $^{66}\text{Ga}^*$  at 30 MeV excitation energy. The respective isospins of the nuclei involved as well as the squares of the Clebsch-Gordan coupling coefficients are indicated. The shaded areas in  $^{65}\text{Ga}$  and  $^{65}\text{Zn}$  correspond to the region of excitation where further particle decay is prohibited.

with  $n_0 = 4$  does not depend very much on the excitation energy, and the enhancement will be strongly damped by the  $(2T_0)^{-2}$  dependence.

The double ratio  $R_B^{CN}(E_{exc})$  for a pure compound nucleus reaction with strict isospin conservation is derived to be

$$R_B^{CN}(E_{exc}) = 1 + (2T_0)^{-2} N^<(E_{exc}) / N^>(E_{exc} - \Delta E_T). \quad (5)$$

$$N^</N^> = N_0^</N_0^> \frac{1 + (2T_0 + 1)^{-1} (\sigma_n^> N_0^> / N_0^< - \sigma_p^<)}{1 - 2(2T_0 + 3)^{-1} \sigma_p^> / \sigma_R - (2T_0 + 1)^{-1} (\sigma_n^> - \sigma_p^< N_0^< / N_0^>) / \sigma_R}, \quad (6)$$

where all terms on the right hand side of Eq. (6) can be calculated by setting  $C^2 \equiv 1$  and separately treating the decay of both isospin systems to  $T^<$  or  $T^>$  levels of the corresponding residual systems. The quantities  $\sigma_n^<$ ,  $\sigma_n^>$ ,  $\sigma_p^<$ , and  $\sigma_p^>$  are the resulting total cross sections for  $p$  and  $n$  emission, and  $\sigma_R = \sigma_p + \sigma_n + \sigma_\alpha$ . The ratio  $N_0^</N_0^>$  can be approximated by the ratio of level densities for  $n$  emission from both isospin systems, respectively, using the expression (iii) given in Sec. III A; it is found that the result does not depend strongly on this ratio since the relation  $N^</N^> \approx (2T_0 + 1) \sigma_R / \sigma_p^< - 1$  holds in the limit  $N_0^</N_0^> \gg 1$ .

### 3. Comparison of theory and experiment

The experimental double ratio  $R[E_{exc}(^{66}\text{Ga}^*)]$  was determined according to Eq. (2). It is fairly insensitive to potential systematic errors (resulting e.g., from target thickness, charge collection,  $\gamma$  detector efficiency, and branching ratios). The targets were separately irradiated in short ( $^{65}\text{Ga}$ ) and long ( $^{65}\text{Zn}$ ) periods. In some cases different excitation energies were reached. Hence for calculating  $R(E_{exc})$ , neighboring data points were linearly interpolated. Experimental error bars were derived from a maximum uncertainty of 9% in each data point. Experimental results and theoretical curves are plotted in Fig. 13.

The dotted curve represents the results for a pure compound nucleus mechanism conserving isospin [Eqs. (5) and (6)]. At 10 MeV  $^3\text{He}$  energy it is  $R \approx 1.4$  and it decreases with increasing energy. For  $E_{^3\text{He}} > 14$  MeV the equilibrium contributions to  $\sigma_p$  and  $\sigma_n$  are smaller than 20% and the PE model predictions have to account for the large double ratio observed. The thin full curve gives the results of the isospin conserving PE model [Eq. (4)] with  $n_0 = 4(2, 2)$ . It is only slightly larger than the corresponding dash-dotted curve for the isospin nonconserving calculation according to Eq. (3), and does not reproduce the high

Here, the quantities  $N^<$  and  $N^>$  are defined as the sums  $N^< = \sum_f C^2(<, f) T_f$  and  $N^> = \sum_f C^2(>, f) T_f$  of the transmission coefficients for all decay channels  $f$ ; they may be calculated from isospin dependent compound nucleus decay codes.<sup>30,32</sup>

It may be interesting to note for codes not containing isospin conservation that the ratio  $N^</N^>$  can be expressed as

experimental value of  $\langle R(26-36 \text{ MeV}) \rangle = 1.92 \pm 0.19$ . This strong enhancement is only matched by PE calculations with a symmetric initial exciton numbers for protons and neutrons. The shaded areas at low excitation energies give the uncertainty due to the influence of the compound nucleus reaction. The lower boundaries for the curves with  $n_0 = 4(1.5, 2.5)$  and  $4(1.75, 2.25)$  and the upper boundary for  $n_0 = 4(2, 2)$  result from combined PE + CN calculations without isospin conservation. The calculations to some extent depend on the effective Coulomb barrier for  $p$  emission from  $^{65}\text{Ga}$  (cf. Fig. 12). Increasing it from 2 to 3 MeV would lower the curve for  $n_0 = 4(1.5, 2.5)$  from  $R = 2.36$  to 2.06 at 34 MeV excitation in  $^{66}\text{Ga}^*$ . With this theoretical uncertainty in mind, the experiment justifies the usual choice<sup>31,35</sup>  $p_{0n} = 1.5$  and  $p_{0p} = 2.5$  for  $^3\text{He}$ -induced reactions, thus confirming the conservation of charge asymmetry in preequilibrium processes

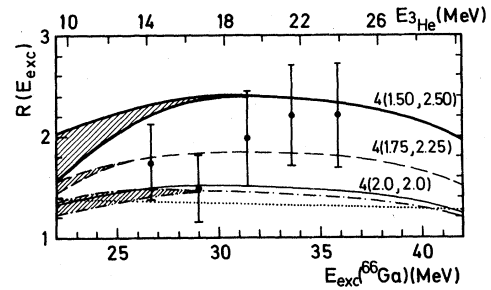


FIG. 13. Comparison of the different theoretical predictions for the double ratio  $R(E_{exc}) = \sigma(^3\text{He}, p) / \sigma(^3\text{He}, n) : \sigma(d, p) / \sigma(d, n)$  with the experimental values (error bars). The dotted curve represents the prediction of the compound nucleus theory with full isospin conservation. The thin full curve corresponds to the isospin conserving PE reaction with symmetric initial exciton numbers  $4(2, 2)$  for the  $^3\text{He}$ -induced reaction. The dash-dot, dash-dash, and the thick full curves give the results of the usual PE model with  $^3\text{He}$  initial exciton numbers equal to  $4(2, 2)$ ,  $4(1.75, 2.25)$ , and  $4(1.5, 2.5)$ , respectively. For the  $d$ -induced reaction the initial configuration  $3(1.5, 1.5)$  was kept fixed.

initiated by these loosely bound projectiles. However, this result is still subject to the uncertainty produced by possible direct transfer contributions which are discussed in Sec. VI.

### V. ISOMERIC CROSS SECTION RATIOS

For the systems (Table III) and projectile energies under investigation, the population of the residual nuclei at low excitation energies is significantly determined by PE decay modes. Therefore, the determination of the ratio  $\sigma_g/\sigma_m$  of cross sections for the population of ground and isomeric state, respectively, with a method similar to that of Huizenga and Vandenbosch,<sup>36</sup> needs some modification,<sup>37</sup> because  $\sigma_g/\sigma_m$  now also reflects the spin distribution following an initial PE emission mode. The model applied here will be presented next, followed by a comparison of its results with our experimental data.

#### A. The model

The statistical model formulation applied to calculate the influence of the initial and intermediate angular momentum distribution on isomer yields is that of Uhl.<sup>38</sup> The initial distribution is assumed to be that of the compound system, i.e.,

$$P(I) = \pi\lambda^2 \sum_{S_P=S_T}^{S_P+S_T} \sum_{l=|I-S_P|}^{I+S_P} \frac{2I+1}{(2S_P+1)(2S_T+1)} T_l(E_P) \quad (7)$$

with the de Broglie wavelength  $\lambda$ , the projectile (target) spin  $S_P$  ( $S_T$ ), the projectile energy  $E_P$ , and the transmission coefficient  $T_l(E_P)$  for the orbital angular momentum  $l$  in the entrance channel.

The sequential decay of this system is described by fully taking into account conservation of parity, angular momentum, and energy. The competing exit channels are those of  $n$ ,  $p$ ,  $d$ ,  $\alpha$ , and  $\gamma$  cascade emission. Equilibrium (EQ) transitions to the states of the corresponding residual nuclei are treated individually at low excitation energies (typically for the first 10–12 discrete levels, with the spectroscopic information taken from Ref. 39), whereas for the continuum region

the level density formula of the back-shifted Fermi gas model has been used:

$$\rho(U, I) = \rho(U) \frac{1}{2\sigma^2} (2I+1) \exp\left[-\frac{I(I+1)}{2\sigma^2}\right], \quad (8)$$

$$\rho(U) = \frac{1}{12(2)^{1/2}} \frac{1}{\sigma a^{1/4}} \frac{\exp\{2[a(U-\Delta)]^{1/2}\}}{(U-\Delta+t)^{5/4}}.$$

Here,  $t$  is the thermodynamic temperature given by

$$U - \Delta = at^2 - t; \quad (9)$$

$a$  and  $\Delta$  are level density parameter and fictive ground state position, respectively, and were taken from Ref. 40. The spin cutoff parameter  $\sigma$  related to the momentum of inertia via

$$\sigma^2 = \frac{\Theta t}{\hbar^2} \quad (10)$$

is referred to as  $\sigma_{\text{Rig}}$  if the rigid body value is taken for  $\Theta$  (with  $r_0 = 1.25$  fm).

Particle decay widths are calculated with optical model transmission coefficients,<sup>19–21,41</sup> decay widths for  $E1$  radiation from  $\gamma$  absorption cross sections by using the Brink-Axel parametrization of the  $E1$  giant dipole resonance,<sup>42</sup> those of radiation with higher multipolarity ( $L \leq 3$ ) from the Weisskopf model normalized to the  $E1$  value. PE emission precedes the first step of the sequential EQ evaporation and depletes the compound nucleus formation. None of the PE decay models now used conserves angular momentum. We assume that (i) the spin and parity population  $d\sigma(E^\pi, U)/dU$  at excitation energy  $U$  of the residual nucleus is that of the EQ population,  $d\sigma^{\text{EQ}}(I^\pi, U)/dU$ , and that (ii) the fractional PE depletion is the same for each partial wave in the entrance channel.<sup>43,44</sup> This leads to<sup>38</sup>

$$\frac{d\sigma(I^\pi, U)}{dU} = [1 - f_{\text{PE}}(E_P)] \frac{d\sigma^{\text{EQ}}(I^\pi, U)}{dU} + \frac{d\sigma_n^{\text{PE}}(U)}{dU} \frac{\frac{d\sigma^{\text{EQ}}(I^\pi, U)}{dU}}{\sum_{I', \pi'} \frac{d\sigma^{\text{EQ}}(I', \pi', U)}{dU}}. \quad (11)$$

TABLE III. Spins and parities of nuclei involved (Ref. 12).

Reaction	$I$ (Target)	$I_g$ (Residual nucleus)	$I_m$ (Residual nucleus)
$^{89}\text{Y}(d, p)^{90}\text{Y}$	$\frac{1}{2}^-$	$2^-$	$7^+$
$^{89}\text{Y}(d, 2n)^{89}\text{Zr}$	$\frac{1}{2}^-$	$\frac{9}{2}^+$	$\frac{1}{2}^-$
$^{93}\text{Nb}(^3\text{He}, n)^{96}\text{Tc}$	$\frac{9}{2}^+$	$\frac{9}{2}^+$	$\frac{1}{2}^-$
$^{93}\text{Nb}(^3\text{He}, 2n)^{94}\text{Tc}$	$\frac{9}{2}^+$	$7^+$	$(2)^+$
$^{93}\text{Nb}(^3\text{He}, 3n)^{93}\text{Tc}$	$\frac{9}{2}^+$	$\frac{9}{2}^+$	$\frac{1}{2}^-$

In Eq. (11),  $d\sigma_x^{PE}(U)/dU$  denotes the energy distribution after PE emission of particles  $x$ . The fraction of interactions leading to nucleon PE emission of type  $x$  is

$$f_{PE}^x(E_P) = \frac{1}{\sigma_R(E_P)} \int_0^{U_{\max}^x} \frac{d\sigma_x^{PE}(U)}{dU} dU, \quad x=n,p \quad (12)$$

with  $\sigma_R(E_P)$  being the optical model reaction cross section. Complex particle PE emission will be neglected so that  $f_{PE}(E_P) = f_{PE}^n(E_P) + f_{PE}^p(E_P)$ . The PE component has been calculated in the framework of the hybrid model<sup>24</sup> with the parameters given in Sec. III.

### B. Comparison with experiment

The experimental results obtained for the reactions  $^{89}\text{Y}(d, 2n)^{89}\text{Zr}^{m,s}$ ,  $^{93}\text{Nb}(^3\text{He}, n)^{93}\text{Tc}^{m,s}$ ,  $^{93}\text{Nb}(^3\text{He}, 2n)^{94}\text{Tc}^{m,s}$ , and  $^{93}\text{Nb}(^3\text{He}, 3n)^{93}\text{Tc}^{m,s}$  are shown in Figs. 14 and 15. All three reactions have in common that the ground state is the high spin state (cf. Table III). Therefore, the ratio  $\sigma_g/\sigma_m$  is expected to increase with projectile energy if Eq. (7) fully applies. The experimental data, however, approach a constant value already at fairly low projectile energies, indicating only a moderate preference of high spin state population. This can be traced back to the PE contribution.

#### 1. $^{93}\text{Nb}(^3\text{He}, 2n)^{94}\text{Tc}$

At low projectile energies the spin population of the initial compound system is almost centered around the target spin [Fig. 16(a)]. The spins of ground state ( $7^+$ ) and isomeric state ( $2^+$ ) of the residual nucleus differ by the same amount from the target spin  $\frac{9}{2}^+$  and we therefore expect an isomeric ratio close to 1 at these energies. The ratio will come out closer to 1 the narrower the initial spin distribution, i.e., the smaller the spin cutoff parameter  $\sigma$ , is. The calculations shown in Fig. 14 confirm these considerations. For projectile energies up to 20 MeV the PE contribution is small ( $f_{PE} \leq 0.2$ ); best agreement is obtained with  $\sigma = 0.7\sigma_{\text{rig}}$ . A similar reduction has been deduced from  $^{93}\text{Nb}(n, 2n)^{92}\text{Nb}^{m,s}$  (Ref. 45) and from the  $^{93}\text{Nb}(n, \alpha)^{90}\text{Y}$  angular distribution.<sup>46</sup>

At higher projectile energies, however, the pure EQ mechanism with  $\sigma \geq 0.5\sigma_{\text{rig}}$  overestimates the isomeric ratio, although the radius parameter  $r_0$  has been given a fairly low value. On the other hand  $\sigma$  is expected to approach  $\sigma_{\text{rig}}$ , because at high excitation energies, effects due to pairing correlations vanish. This discrepancy is reduced by introducing the PE decay mode. A

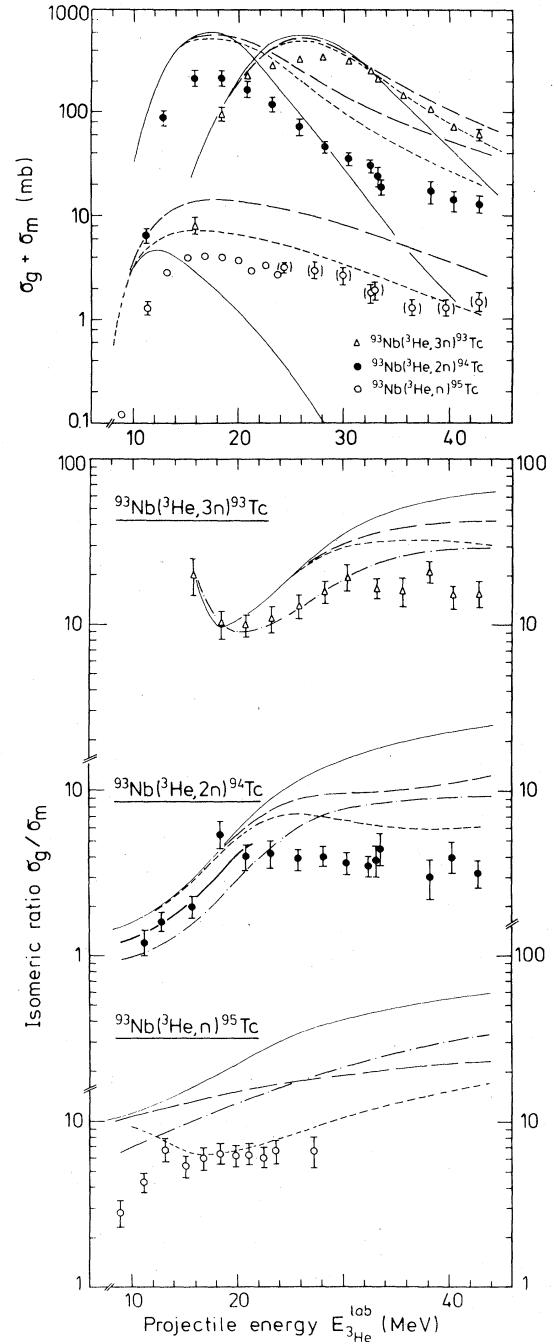


FIG. 14. Excitation functions and isomer ratios for  $^{93}\text{Tc}^{s,m}$ ,  $^{94}\text{Tc}^{s,m}$ , and  $^{95}\text{Tc}^{s,m}$  production in reactions of  $^3\text{He}$  with  $^{93}\text{Nb}$ . Experimental results: this work. Calculations: pure EQ mechanism with  $\sigma/\sigma_{\text{rig}}=1.0$  (thin solid line), 0.7 (thick solid line), 0.5 (dash-dotted); PE competition included with  $\sigma/\sigma_{\text{rig}}=1.0$  and the spin distribution of Eq. (11) (long dashed line), or enhanced angular momentum depletion (short dashed).

considerable fraction of the nucleons emitted ( $f_{PE} \geq 0.5$  for  $E_{^3\text{He}} \geq 40$  MeV) then populates  $^{95}\text{Tc}$  at low excitation; the emission of high energy

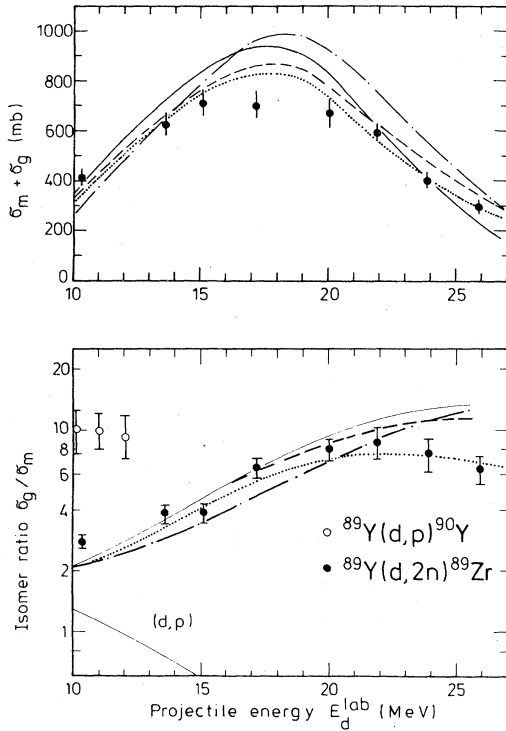


FIG. 15. Same as Fig. 14 for  $^{90}\text{Y}^{\delta,m}$  and  $^{89}\text{Zr}^{\delta,m}$  production in reactions of deuterons with  $^{89}\text{Y}$ . Data for  $^{89}\text{Y}(d,p)$  are from Ref. 29.

neutrons removing several units of angular momentum [compare Figs. 16(a) and 16(b)] is enhanced and so is the relative yield for the low spin isomer. A similar shift is obtained by a substantial reduction of  $\sigma$  [cf. Fig. 16(c)].

## 2. $^{93}\text{Nb}(^3\text{He},3n)^{93}\text{Tc}$ and $^{93}\text{Nb}(^3\text{He},n)^{95}\text{Tc}$

The ground state spin value for  $^{93}\text{Tc}$  is identical with that of the target ( $\frac{9}{2}^+$ ) and exceeds that of the isomeric state by four units of  $\hbar$ . Therefore, the isomeric ratio for  $(^3\text{He}, 3n)$  will generally be higher than that for the  $(^3\text{He}, 2n)$  reaction. At projectile energies  $E_{^3\text{He}} < 20$  MeV the ratio is essentially determined by the individual discrete level sequence in the residual system, because the reaction threshold is at 13.3 MeV and the first excited state populating the isomeric state is at 1.4 MeV. These features are well reproduced by the model calculation applying  $\sigma = 0.7\sigma_{\text{rig}}$  and PE competition.

For  $(^3\text{He}, n)$  the spin situation is the same as for  $(^3\text{He}, 3n)$ , cf. Table III. One might therefore expect well above the reaction threshold a similar energy dependence of the isomeric ratios. Figure 14, however, shows that the ratios differ by more than a factor of 2. In addition, the EQ calculations for  $(^3\text{He}, n)$  fail to reproduce the ratio

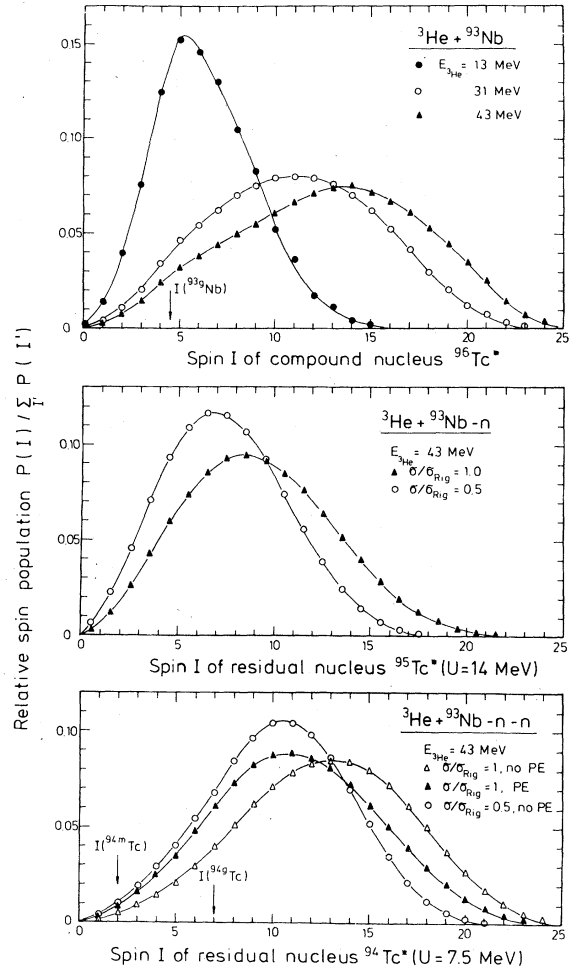


FIG. 16. Normalized populations of (a) positive parity states of the initial compound system  $^3\text{He} + ^{93}\text{Nb}$  for different projectile energies [cf. Eq. (7)]; (b) the same system (for  $E_{^3\text{He}} = 43$  MeV) after emission of one neutron with the spin distribution given by Eq. (11); (c) the residual system  $^{94}\text{Tc}^*$  after sequential neutron (and gamma) emission at  $U = 7.5$  MeV, i.e., below the neutron emission threshold ( $S_n = 8.6$  MeV).

and exceed the experimental result considerably. Inclusion of the PE decay mode improves the calculation in shape, but not in absolute values.

Due to lack of spectroscopic information on  $^{93}\text{Nb}(^3\text{He}, n)$  to low lying states in  $^{95}\text{Tc}$ , no explanation can be offered for the increasing discrepancy below  $E_{^3\text{He}} = 10$  MeV, where the PE fraction  $f_{\text{PE}}$  is well below 0.1, except a possible contribution of the  $(^3\text{He}, n)$  stripping reaction to low spin states (see Sec. VI).

## 3. $^{89}\text{Y}(d,2n)^{89}\text{Zr}$ and $^{89}\text{Y}(d,p)^{90}\text{Y}$

Here the initial population of the compound system due to the low target spin value of  $\frac{1}{2}$  and the light projectile, is concentrated at low spin

values for very low projectile energies  $E_d$ , favoring the transition to  $^{89m}\text{Zr}$  in the  $(d, 2n)$  reaction. With increasing  $E_d$  the spin distribution extends to higher spins and the isomeric ratio therefore increases too. At highest projectile energies the introduction of PE deexcitation again improves the model calculation, but still fails to reproduce the shape of the isomeric ratio at high energies, cf. Fig. 15.

In contrast to the isomer ratios discussed so far, the reaction  $^{89}\text{Y}(d, p)^{90}\text{Y}^{m,s}$  shows a strong preference for the low spin state. The production cross section for the  $7^+$  isomer remains almost constant up to  $E_d = 25$  MeV (Fig. 15). Therefore, the isomer ratio is not expected to change in this energy range by more than one order of magnitude, which is necessary to make experiment and calculation (Fig. 15) comparable. This observation was interpreted by Riley *et al.*<sup>29</sup> with a dominant stripping mechanism. Indeed, Lins *et al.*<sup>47</sup> have shown that in  $^{89}\text{Y}(d, p)^{90}\text{Y}$  the neutron predominantly is transferred to low spin states ( $s_{1/2}, d_{3/2}, d_{5/2}$ ) that populate the  $2^-$  ground state by  $\gamma$  deexcitation.

#### 4. Spin distribution after PE decay

What is the origin of the discrepancies remaining at high projectile energies, in particular for the isomeric ratios for the  $(^3\text{He}, n)$ ,  $(^3\text{He}, 2n)$ , and  $(d, 2n)$  reaction? If, for the moment, the angular momenta of the second and third neutron evaporation may be neglected, it must rest on a difference in the dominant reaction mechanism for the emission of the first neutron. The insert in Fig. 14 emphasizes that the isomeric ratio for  $(^3\text{He}, n)$  almost exclusively reflects the spin distribution after direct and PE neutron emission. In agreement with the tendency observed for  $(^3\text{He}, 2n)$  and  $(^3\text{He}, 3n)$ , we must conclude that the PE (and direct, if present) decay modes favor low spin states even more than assumed in Eq. (11). What then could replace assumption (i) of Sec. 5 A leading to this equation?

Here we suggest<sup>50</sup> implementing one feature of nucleon PE emission, namely its forward peaked angular distribution, to give an estimate of the spin  $\vec{I} = \vec{S}_p + \vec{S}_T + \vec{I}_p - \vec{S}_n - \vec{I}_n$  remaining in the residual system. Forward peaking means that  $\vec{I}_p$  is parallel to  $\vec{l}_n$ , so that approximately  $I = l_p - l_n$ , if the spins of the particles involved are neglected. Herein  $l_n$  is calculated from  $l_p$  and the linear momenta of projectile  $\vec{p}_p$ , and neutron  $\vec{p}_n$ , assuming a fixed impact parameter:  $l_p \approx \vec{p}_p \times \vec{r}_p = l_n \vec{h} / p_n$  or  $l_n = l_p p_n / p_p$ . The spectral distribution of  $p_n$  calculated from  $d\sigma_n^{\text{PE}}(U)/dU$  determines the spectral distribution of  $l_n$ . Assumption (ii) of Sec. V A remains unmodified.

The resulting isomeric ratios and excitation functions are shown in Figs. 14 and 15, too. Considerable improvement is obtained in the regions where PE decay plays an important role. This indicates that the assumption of a spin distribution for PE emission identical with that of an evaporation process may be wrong due to restrictions on the accessible residual states and therefore in favor of too much angular momentum remaining in the system that cannot be carried away by subsequent particle evaporation.

## VI. COMPETING REACTION MECHANISMS

The analysis of excitation functions for loosely bound projectiles so far has been performed in terms of equilibrium and preequilibrium processes. However, the analysis is not unique due to the presence of other direct or nonequilibrium mechanisms such as inelastic scattering of the projectile, particle transfer reactions, etc., some of which show up in "subthreshold" cross sections of (particle,  $xny$ ) reactions i.e., in the emission of complex particles having lower  $Q$  values (see e.g., Fig. 9). The observed high energy tails in excitation functions for  $\alpha$  emission (Figs. 7 and 11) also clearly show the importance of preequilibrium emission of complex particles—yet codes accounting for it in multiparticle decay cascades are still lacking. However, complex particle emission should play a minor role above the threshold for the corresponding multinucleon emission processes.

Another mode of multinucleon emission reaction must also be discussed—the inelastic breakup of the projectile. Hereby, one of the breakup partners (e.g., a neutron) is absorbed by the target nucleus. The excited secondary composite system may further decay by neutron or proton emission and thus contribute to the (particle,  $xn$ ) as well as (particle,  $pxn$ ) excitation functions. Hence, the inelastic breakup bumps observed in particle spectra do contribute to excitation functions in a smooth way while the elastic part reduces the flux into other nonelastic channels. In recent investigations of  $d$ - and  $^3\text{He}$ -induced breakup reactions<sup>48,49</sup> it was found that this inelastic breakup mode normally dominates over the elastic one by a factor of 3 to 5. In the  $d$ -induced breakup this incomplete fusion mode accounts for about 5% of the total reaction cross section at  $A = 60-90$ , i.e., it may contribute 200 to 300 mb to  $(d, pxn)$  reactions if we neglect further charged particle emission. In the measurements of Ref. 48 it was also found that the inelastic  $(d, d'X)$  reaction sums up to about 200 mb at 25.5 MeV bombarding energy. Thus, a

considerable part of the relative large  $^{89}\text{Y}(d, p2n)$  yield may be due to inelastic scattering and breakup of the projectile and might explain part of the discrepancy between theory and experiment for the  $(d, 3n)$  and  $(d, p2n)$  reactions (cf. Sec. III and Fig. 7). The inelastic breakup of the  $^3\text{He}$  projectile is more difficult to deal with since the noninteracting particle(s) may be one of the following six fragments:  $d$ ,  $p$ ,  $n$ ,  $2p$ ,  $pn(T=0)$ ,  $pn(T=1)$ . Up to now only the  $(^3\text{He}, dX)$  reaction has been investigated<sup>49</sup> showing an inelastic contribution of the same order of magnitude as in the case of the  $(d, pX)$  breakup.

Competitive reactions to single nucleon pre-equilibrium emission are transfer reactions to bound states. In particular, neutron transfer reactions occur already below the Coulomb barrier of the projectile so that for lower bombarding energies this mode may dominate. An example is the  $^{89}\text{Y}(d, p)^{90}\text{Y}^{m,s}$  reaction as discussed in Secs. III and V. For the  $^{63}\text{Cu} + ^3\text{He}$  and  $^{64}\text{Zn} + d$  reactions the Coulomb barriers are lower, and the preequilibrium emission of charged particles (i.e., protons) should be considerably enhanced as compared to the  $A=90$  mass region. In this context the question has to be discussed to what extent the isospin conserving direct transfer reactions alone could give rise to the observed enhancement of  $\sigma(^3\text{He}, p)/\sigma(^3\text{He}, n)$  as compared with the ratio  $\sigma(d, p)/\sigma(d, n)$ . As demonstrated in Fig. 12 practically only  $T^<$  states in  $^{65}\text{Ga}$  and  $^{65}\text{Zn}$  contribute to the observed reactions. The  $T^>$  states in both nuclei, which can be populated by the  $^3\text{He}$  induced reaction, decay to the  $T^<$  states of  $^{64}\text{Zn}$  by isospin allowed proton and first forbidden neutron transitions, respectively. Still, the  $(^3\text{He}, p)$  reaction to  $T^<$  states in  $^{65}\text{Zn}$  may proceed via stripping of a proton-neutron pair in the relative  $T=1$  or  $T=0$  state in comparison to the  $T=1$  transition in the  $(^3\text{He}, n)$  reaction. However, the normalization of both  $(^3\text{He}, p)$  transition amplitudes by the factor  $2^{1/2}$  (cf. Ref. 52) prevents a relative enhancement of the  $(^3\text{He}, p)$  to the  $(^3\text{He}, n)$  reaction regarding a specific two-particle state with spins  $j_1$  and  $j_2$  coupled to the total spins  $J$ . Nevertheless, one strong statistical argument remains in favor of the  $(^3\text{He}, p)$  reaction: The  $T=0$ ,  $S=1$  transition may reach even *and* odd  $J$  states of a two-particle multiplet whereas from purity arguments only even *or* odd  $J$  states are excited in the  $T=1$ ,  $S=0$  transitions of  $(^3\text{He}, p)$  and  $(^3\text{He}, n)$  reactions. Therefore, it cannot be excluded that direct reactions could also explain the large double ratio  $R$  as defined in Eq. (2), though their dominance over usual preequilibrium reactions would rather show up in initial exciton numbers  $n_0(d)=2$  and  $n_0(^3\text{He})=3$ , i.e., the number

of particles in the projectile, in contrast to the experimental findings in Secs. III and IV.

On the whole, the extracted numbers of the initial degree of freedom are consistent with the results of analyses of continuous nucleon spectra in  $d$ - and  $^3\text{He}$ -induced reactions near  $A=60$ .<sup>31,35</sup> Yet it is obvious that these determinations of initial exciton numbers take care of some of the direct reaction modes mentioned in an averaging way and hence should not be taken too literally.

## VII. CONCLUSION

The present work contains a systematic survey on reactions induced by the loosely bound  $d$  and  $^3\text{He}$  projectiles for targets in the  $A=60-90$  mass region. From the analysis of the measured excitation functions by equilibrium and preequilibrium models the following general conclusions can be drawn:

- (1) In comparison to the simple Weisskopf-Ewing model, the inclusion of  $\gamma$ -ray competition and angular momentum conservation only slightly improves the agreement with the data. Using experimental separation energies, both approaches well describe thresholds and maxima, but the high energy tails for few particle emission processes are only explained by preequilibrium decay.
- (2) The study of the decay of  $^{66}\text{Ga}^*$  formed by  $d$ - and  $^3\text{He}$ -induced reactions similarly shows that typical entrance channel effects are smeared out as more particles are emitted. The charge distributions of the initial exciton particles in both entrance channels can only be determined from the comparison of single proton and neutron emission yields. From the hybrid model analysis of all data, the initial set of exciton numbers  $n_0(p_{on}, p_{op})$  were found to be  $3(1.5, 1.5)$  for  $d$ -, and  $4(1.5, 2.5)$  for  $^3\text{He}$ -induced reactions.
- (3) Near  $A=90$  for both types of projectiles, the pure Hauser-Feshbach calculation only accounts for the observed isomeric ratios where emission from an equilibrated system dominates. The inclusion of PE emission—assuming the same spin distribution as calculated for equilibrium emission—considerably improves the overall fit. The remaining discrepancy indicates that PE particles carry away more angular momentum than equilibrium particles. This feature could be accounted for in a simple and qualitative approach and should be taken care of in more refined models of PE emission.
- (4) Improved codes should also contain pairing and shell effects in level density calculations. This neglect of the present preequilibrium codes may explain the observed over and underestima-

tion of yields for even-even and doubly odd residual nuclei, respectively.

(5) At present, it seems difficult to include competing direct reaction modes in the analysis of excitation functions (cf., however, Ref. 51). With respect to processes involving complex particle emission, they are dominant below and near thresholds for respective multinucleon emission. Hence, in the analysis of initial exciton numbers from excitation functions as well as from particle spectra, it is not possible to clearly distinguish preequilibrium processes from other direct reactions.

On the whole one might say that also for loosely bound projectiles at bombarding energies up to 45 MeV, the simple Weisskopf-Ewing approach to equilibrium and preequilibrium nucleon emis-

sion—as represented by the OVERLAID ALICE code—yields reasonable fits to a large variety of excitation functions with rather few input parameters.

#### ACKNOWLEDGMENTS

The authors of the University of Bonn are grateful to Dr. T. Mayer-Kuckuk for his continuous interest and support. One of the authors (J.R.R.) wishes to acknowledge the receipt of a fellowship from the Heinrich-Hertz-Stiftung. Another author (M.K.) is indebted to the Otto-Benecke-Stiftung for a grant. This work was supported by the Bundesministerium für Forschung und Technologie.

\*Now at Scientific Control Systems (SCS), Hamburg.

<sup>1</sup>M. Blann, *Annu. Rev. Nucl. Sci.* **25**, 123 (1975) and further references therein.

<sup>2</sup>H. R. Georgi, Ph.D. thesis, University of Hamburg (1977).

<sup>3</sup>H. Strohe, Staatsexamensarbeit, University of Bonn (1978).

<sup>4</sup>M. Kaba, Ph.D. thesis, University of Bonn (1978).

<sup>5</sup>S. N. Ghoshal, *Phys. Rev.* **80**, 939 (1950).

<sup>6</sup>C. Kalbach, *Z. Phys. A* **283**, 401 (1977).

<sup>7</sup>C. F. Williamson, J. P. Boujot, and J. Picard, Centre d'Etudes Nucléaires de Saclay Report No. CEA-R3042 (1966).

<sup>8</sup>C. Tschalár, *Nucl. Instrum. Methods* **61**, 141 (1968).

<sup>9</sup>M. Bormann, H.-K. Feddersen, H.-H. Hölscher, W. Scobel, and H. Wagoner, *Z. Phys. A* **277**, 203 (1976).

<sup>10</sup>S. Flach, Ph.D. thesis and Report No. KFK 2279, Karlsruhe (1976).

<sup>11</sup>G. Erdtmann and W. Soyka, KFA Jülich Report No. Jül-1003-AC (1974).

<sup>12</sup>*Nuclear Data Sheets*, Nucl. Data Project ORNL (Academic, New York, 1978).

<sup>13</sup>A. A. C. Klaasse and P. F. A. Goudsmit, *Z. Phys.* **266**, 75 (1974).

<sup>14</sup>E. A. Bryant, D. R. F. Cochran, and J. P. Knight, *Phys. Rev.* **130**, 1512 (1963).

<sup>15</sup>N. W. Golchert, J. Sedlet, and D. G. Gardner, *Nucl. Phys.* **A152**, 419 (1970).

<sup>16</sup>V. F. Weisskopf and D. H. Ewing, *Phys. Rev.* **57**, 472 (1940).

<sup>17</sup>M. Blann, OVERLAID ALICE, US ERDA Report No. COO-3494-29, 1976 (unpublished).

<sup>18</sup>A. H. Wapstra and N. B. Gove, *Nucl. Data Tables* **9**, 267 (1971).

<sup>19</sup>F. Becchetti and G. Greenlees, *Phys. Rev.* **182**, 1190 (1969).

<sup>20</sup>F. D. Becchetti and G. W. Greenlees, in *Polarization Phenomena in Nuclear Reactions*, edited by H. H. Bartschall and W. Haerberli (The University of Wisconsin Press, Madison, 1971), p. 682.

<sup>21</sup>L. McFadden and G. R. Satchler, *Nucl. Phys.* **84**, 177 (1966).

<sup>22</sup>W. D. Myers and W. J. Swiatecki, *Nucl. Phys.* **81**, 1 (1966).

<sup>23</sup>M. Uhl, *Acta Phys. Austriaca* **31**, 245 (1970); M. Uhl, *Nucl. Phys.* **A184**, 253 (1972).

<sup>24</sup>M. Blann, *Phys. Rev. Lett.* **27**, 337 (1971); **27**, 1550 (1971); **28**, 757 (1972).

<sup>25</sup>J. Ernst and J. Rama Rao, *Z. Phys.* **A281**, 129 (1977).

<sup>26</sup>M. Blann, *Phys. Rev. C* **17**, 1871 (1978) and further references given therein.

<sup>27</sup>E. Gadioli, E. Gadioli Erba, and G. Tagliaferri, *Phys. Rev. C* **17**, 2238 (1978) and further references given therein.

<sup>28</sup>T. Ericson, *Adv. Phys.* **9**, 425 (1960).

<sup>29</sup>C. Riley and B. Linder, *Phys. Rev.* **134**, B559 (1964).

<sup>30</sup>H. L. Harney, H. A. Weidenmüller, and A. Richter, *Phys. Rev. C* **16**, 1774 (1977).

<sup>31</sup>A. Chevarier, N. Chevarier, A. Demeyer, G. Hollinger, P. Pertosa, A. Alevra, R. Dumitrescu, I. R. Lukas, M. T. Magda, and M. E. Nistor, *Nucl. Phys.* **A231**, 64 (1974).

<sup>32</sup>C. Kalbach-Cline, J. R. Huizenga, and H. K. Vonach, *Nucl. Phys.* **A222**, 405 (1974); C. Kalbach, S. M. Grimes, and C. Wong, *Z. Phys.* **A275**, 175 (1975).

<sup>33</sup>R. L. Feinstein, *Ann. Phys. (N.Y.)* **107**, 222 (1977).

<sup>34</sup>W. J. Courtney and J. D. Fox, *At. Data Nucl. Data Tables* **15**, 141 (1975).

<sup>35</sup>J. Bisplinghoff, J. Ernst, R. Löhr, T. Mayer-Kuckuk, and P. Meyer, *Nucl. Phys.* **A269**, 147 (1976).

<sup>36</sup>R. Vandenbosch and J. R. Huizenga, *Phys. Rev.* **120**, 1313 (1960).

<sup>37</sup>C. L. Branquinho, S. M. A. Hoffmann, G. W. Newton, V. J. Robinson, H. Y. Wang, and I. S. Grant, *J. Inorg. Chem.* **41**, 617 (1979).

<sup>38</sup>M. Uhl, Proceedings of the Consultants Meeting on the Use of Nuclear Theory in Neutron Data Evaluation, Vienna, 1976, IAEA-190, p. 361.

<sup>39</sup>*Tables of Isotopes*, edited by C. M. Lederer and V. S. Shirley, 7th edition (Wiley, New York, 1978).

<sup>40</sup>W. Dilg, W. Schantl, H. Vonach, and M. Uhl, *Nucl.*

- Phys. A217, 269 (1973).
- <sup>41</sup>D. Wilmore and P. E. Hodgson, Nucl. Phys. 55, 673 (1964).
- <sup>42</sup>P. Axel, Phys. Rev. 126, 671 (1962).
- <sup>43</sup>J. Gilat, A. Fleury, H. Delagrange, and J. M. Alexander, Phys. Rev. C 16, 694 (1977).
- <sup>44</sup>H. Sakai, H. Ejiri, T. Shibata, Y. Nagai, and K. Okada, Phys. Rev. C 20, 464 (1979).
- <sup>45</sup>M. Bormann, H. H. Bissem, E. Magiera, and R. War-nemünde, Nucl. Phys. A157, 481 (1970).
- <sup>46</sup>M. Bormann, W. Schmidt, V. Schröder, W. Scobel, and U. Seebeck, Nucl. Phys. A186, 65 (1972).
- <sup>47</sup>W. Lins, J. Ernst, N. Takahashi, E. Grosse, and D. Proetel, Nucl. Phys. A179, 16 (1972).
- <sup>48</sup>J. Pampus, J. Bisplinghoff, J. Ernst, T. Mayer-Kuc-kuk, J. Rama Rao, G. Baur, F. Rösel, and D. Traut-mann, Nucl. Phys. A311, 141 (1978).
- <sup>49</sup>J. Bisplinghoff, J. Ernst, J. Kleinfeller, T. Mayer-Kuckuk, G. Baur, and R. Shyam, Contributions to the International Symposium on Continuum Spectra in Heavy Ion Reactions, San Antonio, Texas, 1979.
- <sup>50</sup>H. H. Bissem, M. D. A. Rahman, and W. Scobel (un-published).
- <sup>51</sup>H. Feshbach, A. K. Kerman, and S. Koonin, Ann. Phys. (N. Y.) 125, 429 (1980).
- <sup>52</sup>N. K. Glendenning, At. Data Nucl. Data Tables 16, 1 (1975).